Article

Polarization-Dependent Fiber Metasurface with Beam Collimating and Deflecting

Yuemin Ma, Di Sang, Yi Lin, Qiang An, Zhanshan Sun and Yunqi Fu *

College of Electronic Science and Technology, National University of Defense Technology,
Changsha 410072, China; mayuemin03@nudt.edu.cn (Y.M.); sangdi@nudt.edu.cn (D.S.); linyi@nudt.edu.cn (Y.L.);
anqiang18@nudt.edu.cn (Q.A.); sunzhanshan11@nudt.edu.cn (Z.S.)
* Correspondence: yunqifu@nudt.edu.cn

Abstract: Metasurfaces can arbitrarily manipulate the amplitude, phase, and polarization of optical fields on subwavelength scales. Due to their arbitrary manipulation and compact size, the metasurface can be well integrated with optical fibers. Herein, we demonstrate a polarization-dependent metasurface using birefringent meta-atoms, which can independently control X- and Y-polarization incident light. Each meta-atom allows for the division of phase into 16 steps ranging from 0 to 2π for both X- and Y-polarization, resulting in 256 nanopillars selected from the meta-atom library to satisfy the required phase. With the different effective refractive indices of the cuboid meta-atoms along the X- and Y-axis, we can achieve collimation of the X-polarization emitted beam from an optical fiber while deflecting orthogonally polarized light. As a result, the proposed metasurface collimates an X-polarized beam with a beam radius of 20 μm at $z = 1$ mm and 43.9 μm at $z = 2$ mm. Additionally, the metasurface can effectively deflect the Y-polarized beam to 36.01°, consistent with the results of the theoretical computation. The proposed metasurface exhibits a deflection efficiency of 55.6% for Y-polarized beams with a relative polarization efficiency of 82.2%, while the efficiency for the X-polarization is 71.4%. Our work is considered a promising application for optical communication, sensing, and quantum measurement.

Keywords: metasurface; birefringence; polarization-dependent; collimation; deflection

1. Introduction

Optical fiber has become a mature and popular light conduction tool, with excellent characteristics such as low loss, strong anti-interference ability, light weight and other advantages. It has achieved remarkable success in the optical sensing and telecommunications industries. Widely employed in the medical sector for manufacturing endoscopes and other imaging devices, optical fiber also serves as the primary medium for transmitting signals and data in the field of communication. Recently, with the development of processing technology, the integration of optical components with optical fibers, known as "lab-on-fiber" technology, provides a powerful platform for device integration and miniaturization. Researchers have integrated optoelectronic functional materials and small-size optical devices into the end face of optical fiber, thereby creating a new optical fiber probe for use in microscale applications. It has gained significant attention across various fields such as sensing [1,2] and endoscopic imaging [3]. Traditional bulky optical components like gradient-refractive-index (GRIN) lenses [4,5], plane-concave lenses [6], and refractive ball lenses [7,8] have been mounted on the end face of the optical fiber to achieve corresponding functions in fiber optic imaging, sensing and light field modulation. There is no doubt that "lab-on-fiber" further expands the application scenarios of optical fibers. However, these traditional optical components are limited in function and occupy significant space for phase accumulation in the process of light propagation.

Fortunately, the emergence of metasurfaces in the last decade have has provided a promising solution to the limitations of traditional optical devices. Metasurfaces are

two-dimensional artificial structures consisting of metal or dielectric. They have drawn significant interest for their exceptional ability to manipulate wavefronts at subwavelength scales [9] and their high degree of freedom, allowing for simultaneous modulation of multiple characteristics of the light field, such as phase, amplitude, polarization, etc. Such versatility has led to numerous applications including metalens [10,11], nonlinear optics [12,13], polarization control [14,15], holography [16,17], and imaging [18]. Furthermore, the exploration of metasurfaces is no longer limited to a single function, but realizes a variety of functions through one metasurface, such as the generation of different holograms for different polarizations [19], the generation of different near field and far field images [20], and so on. However, most of these metasurfaces are discrete devices without integration with the light sources. The characteristics of the metasurfaces structure and material, in conjunction with the high aspect ratio and planar cross-section of the optical fiber, promote the emergence of fiber metasurface which represents a novel form of "lab-on-fiber". The principal processing techniques employed for fiber-loaded metasurfaces include focused ion beam (FIB) milling, electron beam lithography (EBL), nano-transfer, and direct laser inscription. The integration of the metasurface with optical fibers brings a disruptive revolution in wavefront modulation engineering, with applications ranging from biosensors [3,21], to optical tweezers [22,23], to optical endoscopes [24,25]. Unlike the discrete metasurfaces, the fiber metasurfaces, as a form of "lab-on-fiber", realize the integration with light sources, and usually only achieve a single or similar function of the light field control [26,27], which limits the original advantages and the development of the fiber metasurface in optics, communications, etc.

Apart from the previously mentioned applications, fiber metasurfaces are also finding applications in emerging domains, such as Rydberg atom-based receivers. In a Rydberg atom-based receiver, two laser beams with wavelengths corresponding to ~852 nm and ~510 nm are employed [28] as the probe laser and the coupling laser, respectively, to prepare cesium (133Cs) Rydberg atoms by the two-photon resonance excitation method. The beam size of the probe laser is crucial in Rydberg atom-based receivers as it affects the average time of Rydberg atoms staying in the interaction volume, which is inversely proportional to the bandwidth of the receiver. Thus, a smaller beam waist of probe laser can effectively increase the instantaneous bandwidth of the receiver [29]. While a structure with a GRIN lens loaded on the end facet of an optical fiber has been proposed for this purpose [30], limitations in GRIN processing technology prevent achieving a beam waist smaller than 300 μm. Nevertheless, the robust wavefront control capacity of metasurfaces makes it possible to generate probe lasers with a narrow beam waist, overcoming the limitations of GRIN lenses. Additionally, maintaining consistent beam polarization between the probe laser and the coupling laser in the vapor cell is crucial to avoid introducing of additional noise and a reducing measurement sensitivity. This is typically achieved using polarization-maintaining fibers to transmit both lasers. However, the cost of polarization-preserving fibers may become prohibitive for the longer lengths required in actual application scenarios. As a cost-effective alternative, single-mode fibers can be employed, but they do not inherently preserve polarization. This presents an opportunity for fiber metasurfaces, which can simultaneously account for beam polarization and diameter modulation, a capability not yet utilized in Rydberg atom-based receivers. By leveraging the wavefront modulation capabilities of metasurfaces, it is possible to enhance the performance of such receivers beyond current limitations.

In this article, we propose a fiber metasurface operating at a wavelength of 852 nm for the independent manipulation of the wavefront of orthogonal linear polarized beams. We set the X-polarization as the desired polarization of the probe laser, while the Y-polarization beam should be deflected to eliminate its effect on the system. By exploiting the birefringence properties of nanopillars, the fiber metasurface achieves beam collimation for X-polarization and deflection for Y-polarization of the optical fiber-emitted beams independently. The target phases obtained by the propagation of the fiber-emitted beam are discretized into 16 steps from 0 to 2π. Then, the corresponding meta-atoms with high

transmission coefficients are selected from the libraries to match the discrete target phases. Full wave simulation results indicate that meta-atoms with a lattice constant of 360 nm and a height of 550 nm can cover the 2π phase modulation range for both X- and Y-polarization. The proposed metasurface effectively collimates the highly divergent Gaussian beam from the optical fiber while deflecting the beam with orthogonal polarization to a 36.01° angle, consistent with the theoretical predictions. The proposed fiber metasurface offers a novel solution for the modulation of probe laser in the Rydberg atom-based receiver, while also simplifying the structure of multifunctional optical devices and expanding the application scenarios of the "lab-on-fiber".

2. Design of the Polarization-Dependent Metasurface

2.1. Design of Birefringent Meta-Atoms

To obtain independent control of orthogonal line polarizations, birefringent rectangular nanopillars are selected as meta-atoms. The transmission matrix of these meta-atoms can be described as [31]

$$T = \begin{bmatrix} t_{xx}e^{i\varphi_x} & 0 \\ 0 & t_{yy}e^{i\varphi_y} \end{bmatrix}, \tag{1}$$

where the elements in the counter-diagonal are 0 because no coupling between X-polarization and Y-polarization is expected in the meta-atoms, t_{xx} is the transmission coefficient of an X-polarized beam, t_{yy} is the transmission coefficient for a Y-polarized one, and φ_x and φ_y represent the accumulated phase resulting from propagation along fast and slow axes within the meta-atoms, respectively, akin to oriented dielectric waveguides. The relevant phases can be expressed as

$$\varphi_{x,y} = 2\pi/\lambda_0 n_{eff\_x,y} d. \tag{2}$$

where n_{eff_x} and n_{eff_y} represent the effective refractive indices for the X-polarized beam and Y-polarized beam, and d is meta-atom height. The non-rotationally symmetric structures exhibit varying equivalent refractive indices for different polarizations of light, and the equivalent refractive indices n_{eff} would change with the geometric parameters of structures. The metasurface realizes independent wavefront shaping for different polarizations on subwavelength scales by introducing distinct phase shifts at the interface between the two media, according to Equations (1) and (2).

In order to achieve the independent modulation for different polarizations, typical cuboid nanopillars made of crystalline silicon (Si) with a refractive index of 3.65 at the wavelength of the probe laser of the Rydberg atom-based receiver are chosen as meta-atoms to realize the birefringence property. The substrate is made up of SiO$_2$ with a refractive index of 1.52 at the operating wavelength as well. As shown in Figure 1, the nanopillars' height of $H = 0.55$ μm is fixed, and the side lengths of the nanopillars W_x and W_y vary from 0.06 μm to 0.32 μm as alternatives for the meta-atoms composing the proposed fiber metasurface. Given that the wavelength of the probe laser required to excite the 113Cs atoms in the vapor cell to become Rydberg atoms in the Rydberg atom-based receiver system is 852 nm, here we set the operating wavelength as 852 nm. The meta-atoms lattice constant of $p = 0.36$ μm, which is smaller than the wavelength in the substrate and greater than the diffraction conditions [32,33], $\lambda_0/2n < p < \lambda_0/n$, where n represents the refractive index of the substrate, to ensure the existence of only zero-order diffraction for normal incidence and only feeble first-order diffraction for the oblique incidence case. The target meta-atoms libraries have been built as shown in Figure 2a,b, which show the transmission coefficients and phase shifts of the meta-atoms for X-polarized beam as the function of W_x and W_y. Figure 2c,d show the transmission coefficients and phase shifts for the Y-polarized beam, which is diagonally symmetric with that for the X-polarized beam incidence. The simulation results show that most of the nanopillars have high transmission coefficients for both X- and Y-polarized beams and phase shifts range from 0 to 2π.
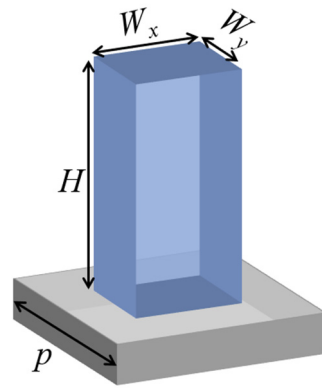
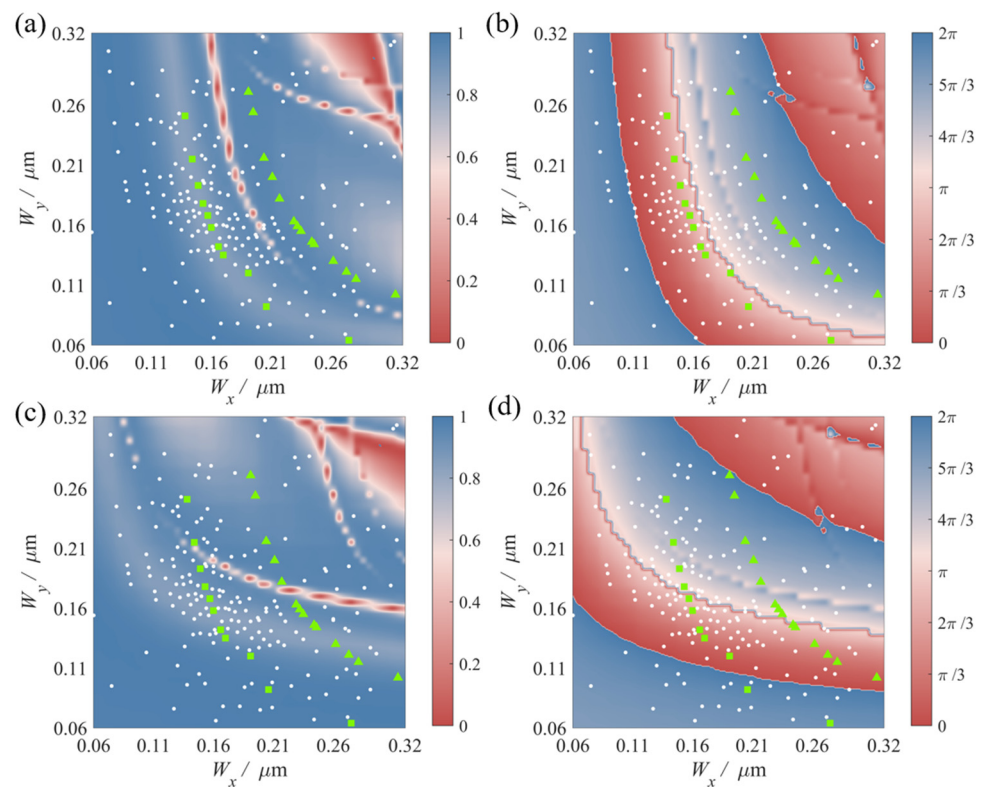**Figure 1.** Schematic of the birefringent meta-atom.

Figure 2. Simulation results of the birefringence meta-atom. (**a**) The transmission coefficients and (**b**) phase shifts of X-polarization. (**c**) The transmission coefficients and (**d**) phase shifts of Y-polarization. The green marks show the selected meta-atoms with phase shifts of $3\pi/4$ and $13\pi/8$ for X-polarization.

2.2. Design of Metasurface

Considering the requirement of the Rydberg atom-based receiver of the probe laser, the metasurface is expected to collimate the X-polarized beam (desired) and deflect the Y-polarized beam (unwanted) of the optical fiber emitted light, as shown in Figure 3. The proposed metasurface aims to realize wavefront modulation of the beam emitted from the single-mode optical fiber SM 780-HP (Nufern, Coherent Inc., Saxonburg, PA, USA). The fundamental mode of a step-index fiber, which is approximated by a Gaussian beam with the beam waist located at the end facet of the fiber [34,35], can be expressed as follows [36]

$$E(r,z) = A_0 \frac{\omega_0}{\omega(z)} e^{-\frac{r^2}{\omega^2(z)}} e^{-i[k(z+\frac{r^2}{2R(z)}-arctg\frac{z}{z_0})]}, \tag{3}$$

where A_0 is the amplitude, ω_0 is the beam waist located in the fiber's end facet, $\omega(z)$ is the beam radius at the axial distance z, $R(z)$ is the radius of curvature, and z_0 is the Rayleigh length. In Equation (3), the phase of the last exponential term is indicative of the divergence of the Gaussian beam. Consequently, in order to realize the collimation of the X-polarization beam after passing through the proposed metasurface, the desired phase should be the opposite of the phase of the fundamental Gaussian mode shown in Equation (3), as illustrated in the following:

$$\varphi_x(x,y,z) = k\left(z + \frac{x^2 + y^2}{2R(z)} - arctg\frac{z}{z_0}\right), \tag{4}$$

where k is the wave number in the medium, z is the propagation distance, (x, y) is the coordinate in the metasurface, $R(z)$ is the curvature radius of the wavefront, z_0 is the Rayleigh length. We set the beam radius of the incident beam as 25 µm which requires a diverging distance of $z = 233.42$ µm to verify the proposed metasurface. The radius of the metasurface is set as 28 µm to leave a margin for the incident beam. Then, the desired phase for the X-polarized beam to realize collimation only is shown in Figure 4a.
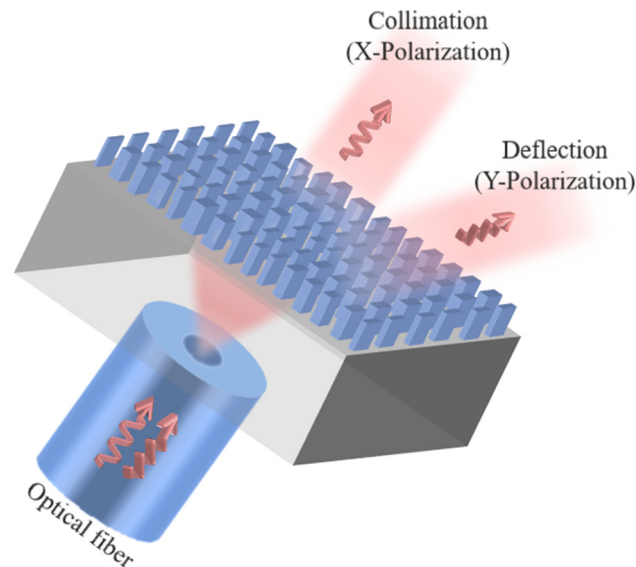

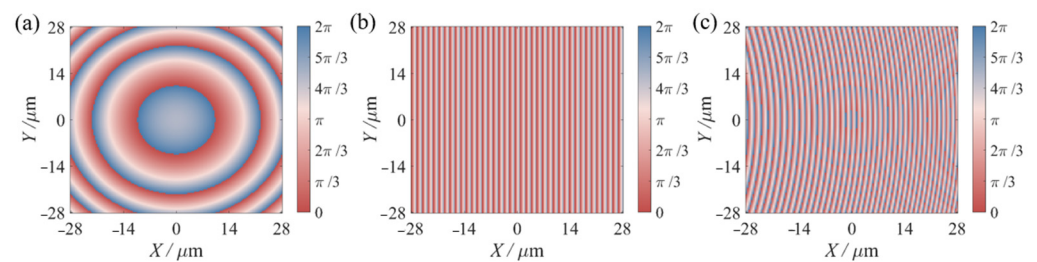**Figure 3.** Schematic of the metasurface's functions.

Figure 4. (**a**) The desired phase for X-polarization. (**b**) The desired phase for Y-polarization's deflection. (**c**) The desired phase for Y-polarization.

In order to obtain beam deflection of the Ypolarization in the X-Z plane, a linear gradient phase along the X-axis should be introduced according to the generalized Snell's law [37]:

$$sin\theta_t n_t - sin\theta_i n_i = \frac{\lambda_0}{2\pi}\frac{d\Phi_y}{dx}, \tag{5}$$

where θ_t is the angle of refraction, θ_i is the angle of incidence, n_t and n_i are the refractive index of the refracted medium and the incident medium, λ_0 is wavelength in free space,

Φ_y is the desired phase of the Y-polarization beam on the metasurface, and $\frac{d\Phi_y}{dx}$ is the phase gradient discontinuity of Y-polarization along the X-axis at the interface. Equation (5) indicates that metasurfaces have the capability to refract beams to arbitrary angles.

To prevent the divergent light of the Ypolarized beam from entering the photodetector behind the vapor cell after interacting with the atom, we also need to apply a collimating phase to make it deflected more thoroughly. For a metasurface, the larger the number of meta-atoms, the better the performance tends to be. Therefore, given of the deflection angle and the number of meta-atom period, we consider four meta-atoms as a big period that should cover the phase from 0 to 2π for the Y-polarized beam and only introduce the gradient phase along the X axis. Thus, the gradient phase is set to $\frac{d\Phi_y}{dx} = \pi/2$. The expected phase of the Y-polarization can be expressed as follows, according to Equations (4) and (5):

$$\varphi_y(x, y, z) = k\left(z + \frac{x^2 + y^2}{2R(z)} - arctg\frac{z}{z_0}\right) + \frac{\pi/2}{p}x, \tag{6}$$

where p is the period of the meta-atom as mentioned before, and x is the abscissa of the proposed metasurface. The first term on the right side of Equation (6) is the collimation phase of Y-polarization, which is in line with that of the X-polarization. The second term is the desired deflection phase changing only along the X axis, which is shown in Figure 4b. Then, the desired phase of the Y-polarized beam is obtained by Equation (6), which is the superposition of the collimation phase and the deflection phase, is demonstrated in Figure 4c. Then, the deflection angle of the Y-polarized beam obtained by Equation (4) is 36.27°, which means the Y-polarized beam can be completely deflected out of the vapor cell at a distance of approximately 2.87 mm from the beam's outgoing surface, according to the structure of the fiber-coupled vapor cell probe in [28]. The collimating phase is also applied to ensure the Y-polarized beam can be completely deflected out of the vapor cell.

The purpose of the proposed metasurface is to collimate the probe laser with X-polarization beam to ensure it has the same polarization as the coupling laser, and acts effectively on the Cs atoms in the vapor cell. However, the Y-polarization beam (unwanted beam) only needs to be excluded from the vapor cell to avoid the sensitivity degradation of the system caused by the introduction of different polarization. To realize the functions of the proposed metasurface efficiently and feasibly, it is discretized from 0 to 2π into 16 discrete phases average with a step size of $\pi/16$. In order to prioritize the probe laser with X-polarization to realize good collimation, we first select meta-atoms with high transmission that satisfy each of the 16 discrete phases of the X-polarization beam, respectively. Then, among these pre-selected meta-atoms, we further refine our selection to those that precisely fulfill the 16 discrete phases of Y-polarization under the premise of satisfying 16 discrete phases of x polarization, respectively. Consequently, the combination of 16 discrete phases of the X-polarized beam and 16 discrete phases of the Y-polarized beam results in a total of 256 phase combinations. This represents the 256 high-transmittance meta-atoms that satisfy the X- and Y-polarized discrete phase responses that are selected from the meta-atom libraries, which is indicated by markers in Figure 2. The squares and triangles in Figure 2 mark the meta-atoms with X-polarization phase shifts of $3\pi/4$ and $13\pi/8$, whose geometric parameters can be found in the library. The white dots indicate the remaining selected meta-atoms with different phase responses. Figure 5a,b illustrates the actual phase responses of the 256 selected meta-atoms to the X- and Y-polarized beam, respectively. The abscissa represents the ideal discrete phase response of the selected meta-atoms and the ordinate means that of the Y-polarized beam. The phases range of the selected meta-atoms spanning from 0 to 2π, are in good accordance with the discrete phases of X-polarization. Due to the priority given to ensuring the alignment of X-polarization, it is inevitable that the phase's responses to the Y-polarization are not as perfect as that of the X-polarization beam. Figure 5c,d show the transmission of the selected meta-atoms to the X- and Y- polarized beam, which illustrates that transmission coefficients of the 256 selected meta-atoms to the both X- and Y-polarization are higher than 81%. As

shown in Figure 6a,b, the phase profile along *x* = 0 of the X-polarization and Y-polarization theoretical phase and discrete matching phase provided by the selected meta-atoms are nearly consistent, respectively. Figure 6c shows the structure of the proposed metasurface obtained by mapping the metasurface's discrete phases to the geometries of the meta-atoms marked in Figure 2.
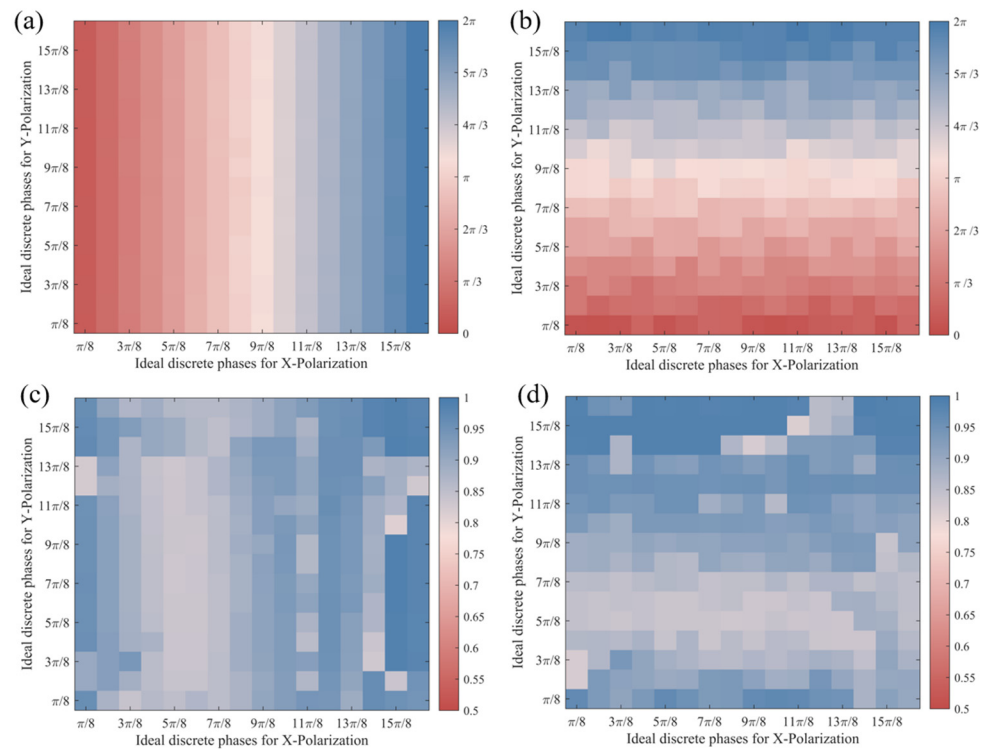

Figure 5. The selected meta-atoms phase responses to the (**a**) X-polarization and (**b**) Y-polarization. The selected meta-atoms transmission to the (**c**) X-polarization and (**d**) Y-polarization.
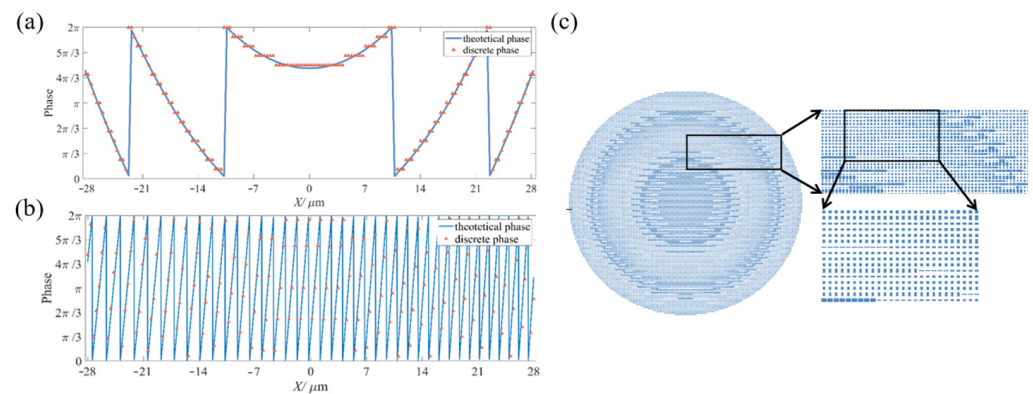

Figure 6. Phase profiles of (**a**) X-polarized beam and Y-polarization beam along *x* = 0. (**b**) Schematic illustration of the metasurface. (**c**) The structure of the proposed metasurface.

3. Results

To verify the functions of the metasurface, the metasurface's structure demonstrated in Figure 6c is simulated by Ansys Lumerical FDTD. The emitted beam from the optical fiber with X- and Y-polarization are imported into software as the incident beam to validate the functions of the proposed metasurface, whose electric field distribution is calculated by Equation (3). Considering the computer memory and the symmetry of X-and Y- polarization desired phases, we utilize symmetric and anti-symmetric boundaries to reduce the simulation region by half, while the remaining boundary conditions are set

to PML. Figure 7a shows the optical fiber emitted beam with Y-polarization is deflected via the proposed metasurface. The far field intensity distribution shown in Figure 8b illustrates that the Y-polarized beam is deflected in the X-Z plane with an angle of 36.01° and unchanged in the Y-Z plane. The practical deflection angle of 36.01° is basically in line with the theoretical result of 36.27° obtained by Equation (5). The error between the theoretical and practical deflection angle is because the proposed metasurface is finite and the phase responses of the meta-atoms which make up the metasurface are not exactly the same as the ideal phase. The wavefront shown in Figure 7c indicates that the optical fiber emitted beam with Y-polarization becomes a plane wave after passing through the proposed metasurface, which means the Y-polarized beam is collimated by the metasurface. And the angle between its wave vector and the incident wave vector is 36.01°, which further proves the proposed metasurface realizes deflection with an envisioned angle. The transmission efficiency of the metasurface to the Y-polarization is 67.8% and the relative deflection efficiency of 82.2%, according to the definition in [38], resulting in an absolute deflection efficiency of 55.7%. These results imply that the proposed metasurface realizes collimation and deflection for the Y-polarized beam simultaneously as designed, which has the capability to reduce the interference of the Y-polarization component of the probe laser on the X-polarization beam component in the vapor cell of the Rydberg atom-based receiver compared with the beam that is not modulated by the metasurface.
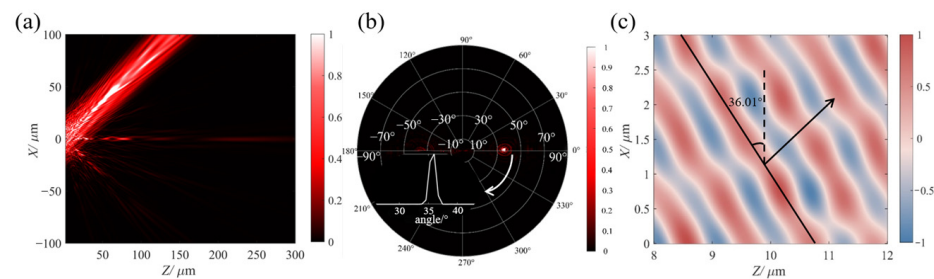

Figure 7. (**a**) Intensity distributions of the deflected beam in the X-Z plane. (**b**) Far-field distribution. (**c**) Wavefront of the deflection beam.
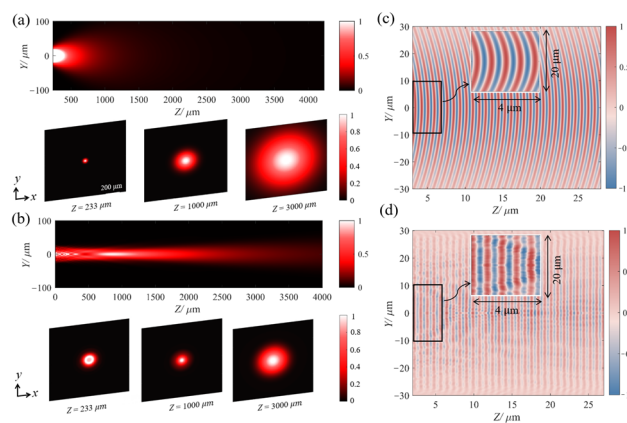

Figure 8. (**a**) Uncollimated divergence of the outgoing light from an optical fiber. (**b**) Intensity distributions of the collimated beam in axial and cross-section. (**c**) Wavefront of the uncollimation beam. (**d**) Wavefront of the collimated beam.

Figure 8a shows the uncollimated beam emitted from the optical fiber in Y-Z plane, and the normalized electric field intensity at three representative positions along the propagation direction, that is, $z = 0.233$ mm, which is the diverging distance of fiber emitted light, $z = 1$ mm and $z = 3$ mm. It can be observed that the beam without collimation by the metasurface diverges rapidly, which extends from a beam radius of 25 μm at $z = 0.233$ mm to a beam radius 106.7 μm at $z = 1$ mm, and that ulteriorly diverges to 319.7 μm at an axial

distance of $z = 3$ mm. Figure 8b demonstrates the illumination intensity of the collimated beam with X-polarization in Y-Z plane and the cross-section electric field intensity of three positions, which is the surface of the proposed metasurface, $z = 1$ mm and $z = 3$ mm. The beam collimated by the metasurface has a beam radius of 25 μm, which is set, then becomes a beam radius of 20 μm at an axial distance of 1 mm, and that further enlarges to a beam radius of 43.9 μm at the axial distance of $z = 3$ mm, implying that the proposed metasurface exhibits excellent collimation function for X-polarized beam. And the intensity of the collimated beam in cross-sections presents a weak distribution around the stronger central intensity, which is still consistent with the Gaussian distribution. The collimated beam can be regarded as a zero-degree deflection, which has a total efficiency of 71.4%. Figure 8c shows the beam emitted from the fiber without collimation is a spherical wave. However, as demonstrated in Figure 8d, the beam collimated by the proposed metasurface appears as a plane wave, which implies that the metasurface designed here realizes collimation for X-polarization effectively with the deflection of the Y-polarized beam.

4. Discussion

In this paper, a multifunctional fiber metasurface is proposed to realize collimation of the X-polarization and deflection of the Y-polarization of the fiber-emitted beam. The introduction of birefringent meta-atoms with different lengths and widths enables the realization of independent modulation of X- and Y-polarization. The required phases for X- and Y-polarizations were obtained from an approximate representation of the Gaussian beam fundamental mode and a gradient phase distribution. In order to achieve the desired function more efficiently, the phase distributions of the two polarizations are discretized to match the meta-atoms with different phase shifts. The nanopillars constituting the bifunctional metasurfaces exhibit phase responses to different polarizations that match the required phases for different polarizations. Additionally, to validate the theoretical design, full-wave simulations are performed to verify the effectiveness of the proposed metasurface. The simulation results demonstrate that the metasurface effectively achieves collimation for the X-polarization with a total efficiency of 74.1%. For the Y-polarization, a beam deflection of 36.01° is achieved with a total efficiency of 55.7% and the relative deflection efficiency is 82.2%. The proposed metasurface realizes the collimation of the small-diameter beam incident into the vapor cell and the selection of the beam's polarization, which satisfies the requirements of the high performance Rydberg atom-based receiver for the probe laser. The proposed metasurface based on a fiber-optic platform is capable of overcoming the limitations of conventional GRIN lenses, including their bulkiness and the unrealizable beam diameter for the beam collimation. In summary, the proposed metasurface not only proposes a novel solution for enhancing the performance of the Rydberg atom-based receiver through beam modulation, but also enriches the functionality of the metasurface based on the optical fiber platform.

Author Contributions: Conceptualization, Y.M., D.S. and Y.L.; Data curation, Y.M. and Z.S.; Resources, Y.M.; Software, Y.M.; Supervision, Q.A. and Y.F.; Writing—original draft, Y.M. and D.S.; Writing—review and editing, Y.M. and D.S. All authors have read and agreed to the published version of the manuscript.

Institutional Review Board Statement: Not applicable.

Informed Consent Statement: Not applicable.

Data Availability Statement: The data presented in this study are available on request from the corresponding author.

References

1. Principe, M.; Consales, M.; Castaldi, G.; Galdi, V.; Cusano, A. Evaluation of fiber-optic phase-gradient meta-tips for sensing applications. *Nanomater. Nanotechnol.* **2019**, *9*, 184798041983272. [CrossRef]
2. Yang, Y.B.; Wang, D.N.; Xu, B.; Wang, Z.K. Optical fiber tip interferometer gas pressure sensor based on anti-resonant reflecting guidance mechanism. *Opt. Fiber Technol.* **2018**, *42*, 11–17. [CrossRef]
3. Pahlevaninezhad, H.; Khorasaninejad, M.; Huang, Y.-W.; Shi, Z.; Hariri, L.P.; Adams, D.C.; Ding, V.; Zhu, A.; Qiu, C.-W.; Capasso, F.; et al. Nano-optic endoscope for high-resolution optical coherence tomography in vivo. *Nat. Photonics* **2018**, *12*, 540–547. [CrossRef]
4. Mao, R.Q.; Lin, Y.; Yang, K.; An, Q.; Fu, Y.Q. A High-Efficiency Fiber-Coupled Rydberg-Atom Integrated Probe and Its Imaging Applications. *IEEE Antennas Wirel. Propag. Lett.* **2023**, *22*, 352–356. [CrossRef]
5. Kasztelanic, R.; Filipkowski, A.; Anuszkiewicz, A.; Stafiej, P.; Stepniewski, G.; Pysz, D.; Krzyzak, K.; Stepien, R.; Klimczak, M.; Buczynski, R. Integrating Free-Form Nanostructured GRIN Microlenses with Single-Mode Fibers for Optofluidic Systems. *Sci. Rep.* **2018**, *8*, 5072. [CrossRef] [PubMed]
6. Guggenheim, J.A.; Li, J.; Allen, T.J.; Colchester, R.J.; Noimark, S.; Ogunlade, O.; Parkin, I.P.; Papakonstantinou, I.; Desjardins, A.E.; Zhang, E.Z.; et al. Ultrasensitive plano-concave optical microresonators for ultrasound sensing. *Nat. Photonics* **2017**, *11*, 714–719. [CrossRef]
7. Zhao, M.T.; Huang, Y.; Kang, J.U. Sapphire ball lens-based fiber probe for common-path optical coherence tomography and its applications in corneal and retinal imaging. *Opt. Lett.* **2012**, *37*, 4835–4837. [CrossRef] [PubMed]
8. Mo, J.H.; Zheng, W.; Huang, Z.W. Fiber-optic Raman probe couples ball lens for depth-selected Raman measurements of epithelial tissue. *Biomed. Opt. Express* **2010**, *1*, 17–30. [CrossRef] [PubMed]
9. Soukoulis, C.M.; Wegener, M. Past achievements and future challenges in the development of three-dimensional photonic metamaterials. *Nat. Photonics* **2011**, *5*, 523–530. [CrossRef]
10. Sang, D.; Xu, M.F.; Pu, M.B.; Zhang, F.; Guo, Y.H.; Li, X.; Ma, X.L.; Fu, Y.Q.; Luo, X.G. Toward High-Efficiency Ultrahigh Numerical Aperture Freeform Metalens: From Vector Diffraction Theory to Topology Optimization. *Laser Photonics Rev.* **2022**, *16*, 2200265. [CrossRef]
11. Zang, X.F.; Xu, W.W.; Gu, M.; Yao, B.S.; Chen, L.; Peng, Y.; Xie, J.Y.; Balakin, A.V.; Shkurinov, A.P.; Zhu, Y.M.; et al. Polarization-Insensitive Metalens with Extended Focal Depth and Longitudinal High-Tolerance Imaging. *Adv. Opt. Mater.* **2020**, *8*, 1901342. [CrossRef]
12. Ahmed, H.; Kim, H.; Zhang, Y.B.; Intaravanne, Y.; Jang, J.; Rho, J.; Chen, S.Q.; Chen, X.Z. Optical metasurfaces for generating and manipulating optical vortex beams. *Nanophotonics* **2022**, *11*, 941–956. [CrossRef]
13. Liu, B.Y.; Sain, B.; Reineke, B.; Zhao, R.Z.; Meier, C.; Huang, L.L.; Jiang, Y.Y.; Zentgraf, T. Nonlinear Wavefront Control by Geometric-Phase Dielectric Metasurfaces: Influence of Mode Field and Rotational Symmetry. *Adv. Opt. Mater.* **2020**, *8*, 1902050. [CrossRef]
14. Zhao, Q.; Yuan, W.; Qu, J.; Cheng, Z.; Peng, G.-D.; Yu, C. Optical Fiber-Integrated Metasurfaces: An Emerging Platform for Multiple Optical Applications. *Nanomaterials* **2022**, *12*, 793. [CrossRef] [PubMed]
15. Ding, F.; Chang, B.; Wei, Q.; Huang, L.; Guan, X.; Bozhevolnyi, S.I. Versatile Polarization Generation and Manipulation Using Dielectric Metasurfaces. *Laser Photonics Rev.* **2020**, *14*, 2000116. [CrossRef]
16. Overvig, A.C.; Shrestha, S.; Malek, S.C.; Lu, M.; Stein, A.; Zheng, C.X.; Yu, N.F. Dielectric metasurfaces for complete and independent control of the optical amplitude and phase. *Light-Sci. Appl.* **2019**, *8*, 92. [CrossRef] [PubMed]
17. Lee, G.Y.; Yoon, G.; Lee, S.Y.; Yun, H.; Cho, J.; Lee, K.; Kim, H.; Rho, J.; Lee, B. Complete amplitude and phase control of light using broadband holographic metasurfaces. *Nanoscale* **2018**, *10*, 4237–4245. [CrossRef] [PubMed]
18. Ren, H.; Jang, J.; Li, C.; Aigner, A.; Plidschun, M.; Kim, J.; Rho, J.; Schmidt, M.A.; Maier, S.A. An achromatic metafiber for focusing and imaging across the entire telecommunication range. *Nat. Commun.* **2022**, *13*, 4183. [CrossRef] [PubMed]
19. Shalaev, M.I.; Sun, J.B.; Tsukernik, A.; Pandey, A.; Nikolskiy, K.; Litchinitser, N.M. High-Efficiency All-Dielectric Metasurfaces for Ultracompact Beam Manipulation in Transmission Mode. *Nano Lett.* **2015**, *15*, 6261–6266. [CrossRef]
20. Liu, M.Z.; Zhu, W.Q.; Huo, P.C.; Feng, L.; Song, M.W.; Zhang, C.; Chen, L.; Lezec, H.J.; Lu, Y.Q.; Agrawal, A.; et al. Multifunctional metasurfaces enabled by simultaneous and independent control of phase and amplitude for orthogonal polarization states. *Light-Sci. Appl.* **2021**, *10*, 107. [CrossRef]
21. Rahman, B.M.A.; Viphavakit, C.; Chitaree, R.; Ghosh, S.; Pathak, A.K.; Verma, S.; Sakda, N. Optical Fiber, Nanomaterial, and THz-Metasurface-Mediated Nano-Biosensors: A Review. *Biosensors* **2022**, *12*, 42. [CrossRef] [PubMed]
22. Saleh, A.A.E.; Sheikholeslami, S.; Gastelum, S.; Dionne, J.A. Grating-flanked plasmonic coaxial apertures for efficient fiber optical tweezers. *Opt. Express* **2016**, *24*, 20593–20603. [CrossRef] [PubMed]
23. Liberale, C.; Minzioni, P.; Bragheri, F.; De Angelis, F.; Di Fabrizio, E.; Cristiani, I. Miniaturized all-fibre probe for three-dimensional optical trapping and manipulation. *Nat. Photonics* **2007**, *1*, 723–727. [CrossRef]
24. Sun, Y.; Wang, C.; Zheng, S.; Tao, X.; Liu, X.; Li, Y.; Wu, F.; Zheng, Z. Double-layer polarization-independent achromatic metasurface array for optical fiber bundle coupling in microendoscope. *Sci. Rep.* **2022**, *12*, 20476. [CrossRef] [PubMed]
25. Xie, N.; Carson, M.D.; Froch, J.E.; Majumdar, A.; Seibel, E.J.; Bohringer, K.F. Large field-of-view short-wave infrared metalens for scanning fiber endoscopy. *J. Biomed. Opt.* **2023**, *28*, 094802. [CrossRef] [PubMed]

26. Ghimire, I.; Yang, J.; Gurung, S.; Mishra, S.K.; Lee, H.W.H. Polarization-dependent photonic crystal fiber optical filters enabled by asymmetric metasurfaces. *Nanophotonics* **2022**, *11*, 2711–2717. [CrossRef]

27. Li, J.; Li, R.; Xue, X.; Jiang, X.; Chen, X.; Chui, H.-C. Achromatic Flat Metasurface Fiber Couplers within Telecom Bands. *Photonics* **2022**, *10*, 28. [CrossRef]

28. Mao, R.Q.; Lin, Y.; Fu, Y.Q.; Ma, Y.M.; Yang, K. Digital Beamforming and Receiving Array Research Based on Rydberg Field Probes. *IEEE Trans. Antennas Propag.* **2024**, *72*, 2025–2029. [CrossRef]

29. Prajapati, N.; Rotunno, A.P.; Berweger, S.; Simons, M.T.; Artusio-Glimpse, A.B.; Voran, S.D.; Holloway, C.L. TV and video game streaming with a quantum receiver: A study on a Rydberg atom-based receiver's bandwidth and reception clarity. *AVS Quantum Sci.* **2022**, *4*, 035001. [CrossRef]

30. Lin, Y.; Wu, F.-C.; Mao, R.-Q.; Yao, J.-W.; Liu, Y.; An, Q.; Fu, Y.-Q. Development of three-port fiber-coupled vapor cell probe and its application in microwave digital communication. *Acta Phys. Sin.* **2022**, *71*, 170702. [CrossRef]

31. Saleh, B.E.; Teich, M.C. *Fundamentals of Photonics*, 2nd ed.; John Wiley & Sons: Hoboken, NJ, USA, 2007.

32. Fan, Z.B.; Shao, Z.K.; Xie, M.Y.; Pang, X.N.; Ruan, W.S.; Zhao, F.L.; Chen, Y.J.; Yu, S.Y.; Dong, J.W. Silicon Nitride Metalenses for Close-to-One Numerical Aperture and Wide-Angle Visible Imaging. *Phys. Rev. Appl.* **2018**, *10*, 014005. [CrossRef]

33. Grann, E.B.; Moharam, M.G.; Pommet, D.A. Optimal design for antireflective tapered two-dimensional subwavelength grating structures. *J. Opt. Soc. Am. A* **1995**, *12*, 333–339. [CrossRef]

34. Yoda, H.; Polynkin, P.; Mansuripur, M. Beam quality factor of higher order modes in a step-index fiber. *J. Light. Technol.* **2006**, *24*, 1350–1355. [CrossRef]

35. Ye, H.; Sun, Q.; Guo, Z.; Hou, Y.; Wen, F.; Yuan, D.; Qin, F.; Zhou, G. Theoretical realization of single-mode fiber integrated metalens for beam collimating. *Opt. Express* **2021**, *29*, 27521–27529. [CrossRef]

36. Marcuse, D. Gaussian approximation of the fundamental modes of graded-index fibers. *J. Opt. Soc. Am.* **1978**, *68*, 103–109. [CrossRef]

37. Yu, N.; Genevet, P.; Kats, M.A.; Aieta, F.; Tetienne, J.P.; Capasso, F.; Gaburro, Z. Light propagation with phase discontinuities: Generalized laws of reflection and refraction. *Science* **2011**, *334*, 333–337. [CrossRef]

38. Egorov, V.; Eitan, M.; Scheuer, J. Genetically optimized all-dielectric metasurfaces. *Opt. Express* **2017**, *25*, 2583–2593. [CrossRef]